

Are gadolinium contrast agents suitable for gadolinium neutron capture therapy?

Gelsomina De Stasio*, Deepika Rajesh[†], Patrizia Casalbore[‡],
Matthew J. Daniels*, Robert J. Erhardt^{*,§}, Bradley H. Frazer*, Lisa M. Wiese*,
Katherine L. Richter^{¶,¶}, Brandon R. Sonderegger*, Benjamin Gilbert^{*,2},
Sebastien Schaub[#], Rachel J. Cannara*, John F. Crawford^{**}, Mary K. Gilles^{††},
Tolek Tyliczszak^{††}, John F. Fowler[†], Luigi M. Larocca^{‡‡}, Steven P. Howard[†],
Delio Mercanti^{§§}, Minesh P. Mehta[†] and Roberto Pallini^{¶¶}

*University of Wisconsin-Madison, Department of Physics and Synchrotron Radiation Center, 3731
Schneider Drive, Stoughton WI 53589, USA

[†]University of Wisconsin, Department of Human Oncology, Madison WI 53792, USA

[‡]Istituto di Biologia Cellulare, CNR, Viale Marx 15, I-00137 Roma, Italy

[§]University of Wisconsin, Department of Statistics, Madison WI 53706, USA

[¶]Bob Jones University, Greenville, SC 29614, USA

[#]Biomedical Engineering Laboratory, PSE-A, Swiss Federal Institute of Technology, CH-1015 Lausanne,
Switzerland

^{**}Hengelweg 37, CH-5303 Würenlingen, Switzerland

^{††}Lawrence Berkeley National Laboratory, 1 Cyclotron Rd. MS 6-2100, Berkeley, CA 94720, USA

^{‡‡}Istituto di Anatomia Patologica, Università Cattolica del Sacro Cuore, Largo A. Gemelli 8, I-00168
Roma, Italy

^{§§}Istituto di Neurobiologia e Medicina Molecolare, CNR, Viale Marx 15, 00137 Roma, Italy

^{¶¶}Istituto di Neurochirurgia, Università Cattolica del Sacro Cuore, Largo A. Gemelli 8, I-00168 Roma, Italy

Objective: Gadolinium neutron capture therapy (GdNCT) is a potential treatment for malignant brain tumors based on two steps: (1) injection of a tumor-specific ¹⁵⁷Gd compound; (2) tumor irradiation with thermal neutrons. The GdNC reaction can induce cell death provided that Gd is proximate to DNA. Here, we studied the nuclear uptake of Gd by glioblastoma (GBM) tumor cells after treatment with two Gd compounds commonly used for magnetic resonance imaging, to evaluate their potential as GdNCT agents.

Methods: Using synchrotron X-ray spectroscopy, we analyzed the Gd distribution at the subcellular level in: (1) human cultured GBM cells exposed to Gd-DTPA or Gd-DOTA for 0–72 hours; (2) intracerebrally implanted C6 glioma tumors in rats injected with one or two doses of Gd-DOTA, and (3) tumor samples from GBM patients injected with Gd-DTPA.

Results: In cell cultures, Gd-DTPA and Gd-DOTA were found in 84% and 56% of the cell nuclei, respectively. In rat tumors, Gd penetrated the nuclei of 47% and 85% of the tumor cells, after single and double injection of Gd-DOTA, respectively. In contrast, in human GBM tumors 6.1% of the cell nuclei contained Gd-DTPA.

Discussion: Efficacy of Gd-DTPA and Gd-DOTA as GdNCT agents is predicted to be low, due to the insufficient number of tumor cell nuclei incorporating Gd. Although multiple administration schedules in vivo might induce Gd penetration into more tumor cell nuclei, a search for new Gd compounds with higher nuclear affinity is warranted before planning GdNCT in animal models or clinical trials. [Neurol Res 2005; 27: 387–398]

Keywords: Gd-DOTA; Gd-DTPA; gadolinium neutron capture therapy (GdNCT); glioblastoma; spectromicroscopy; synchrotron

INTRODUCTION

Gadolinium neutron capture therapy (GdNCT) is a potential treatment for malignant brain tumors. The

Correspondence and reprint requests to: Gelsomina De Stasio, University of Wisconsin-Madison, Department of Physics and Synchrotron Radiation Center, 3731 Schneider Drive, Stoughton WI 53589, USA. [pupa@src.wisc.edu] Accepted for publication October 2004.

¹Present address: Department of Chemistry and Biochemistry, University of Notre Dame, IN 46556, USA.

²Present address: Department of Earth and Planetary Science, University of California, Berkeley CA 94708, USA.

GdNCT concept, which has not yet been clinically tested, is based on two steps: (1) the patient is injected with a tumor-specific ¹⁵⁷Gd compound; (2) the tumor is irradiated with thermal or epithermal neutrons. After neutron capture, the ¹⁵⁸Gd excited nucleus decays, delivering localized irradiation. Both the injection of the Gd compound and thermal neutron irradiation result in only limited damage to normal brain, while the radiation dose is considerably higher in the Gd-containing tumor. This is due to the high neutron absorption cross

section (i.e. the probability that an element may capture a neutron) of the ^{157}Gd isotope. The absorption cross section is 254,000 barn for ^{157}Gd , compared with values of 0–2 barn for hydrogen, nitrogen and oxygen, or any other element physiologically present in the brain, and 3840 barn for boron, the element most commonly employed to date.

Why GdNCT?

Glioblastoma multiforme (GBM) affects 12,000 patients/year in the US, and an estimated 300,000 patients worldwide. The incidence and mortality are almost equal, indicating the uniformly fatal outcome of this brain malignancy, and the need for new therapeutic approaches. The vast majority of GBM patients succumb within 1 year of diagnosis. Conventional therapy consists of maximal resection followed by post-operative radiotherapy to ~ 60 Gy, with a median survival of just under 10 months.

Although molecular biology-based therapeutic approaches are the major focus of current clinical research efforts, a more immediate impact might be obtained by developing a safe radiation dose-escalation strategy. GdNCT represents one such novel approach.

Although the idea of Gd-based NCT was first formulated in the 1980s^{1,2} as an alternative to a similar therapy based on ^{10}B ³, its development has suffered due to lack of appropriate Gd-containing tumor-selective agents⁴. Conventional Gd compounds localize in and around the abnormal vasculature surrounding tumors, as shown by MRI. To date, it has been surmised that this Gd remains extracellular, relative to the malignant neoplasm itself. Until recently, sophisticated techniques to analyze the microscopic distribution of Gd, and correlate it with the location of cell nuclei were not available. We recently showed that a Gd-containing MRI contrast agent (Gd-DTPA) penetrates cancer cell nuclei *in vitro*⁵, thereby stimulating a reevaluation of the GdNCT approach.

The complete neutron capture reaction

When a neutron is captured by ^{157}Gd , a highly localized nuclear reaction occurs producing five Auger and Coster-Kronig (ACK) electrons, 0.7 internal conversion electrons, 1.8 X-rays and 0.8 X-rays, with varying energies and radiation lengths (for more details on GdNC nuclear reaction see^{6–11}). Among these, the most abundant and most biologically relevant are the high linear-energy-transfer (LET) ACK electrons. These range in energy between 0 and 50 keV with an average of 4.2 keV and average LET of 0.3 MeV/ μm . By comparison, in boron neutron capture therapy the average LET is 0.2 MeV/ μm for both Li and alpha particles.

However, the range (or mean free path) of ACK electrons is limited to 0–150 nm (12.5 nm for the average energy of 4.2 keV)^{6,7}. Due to this rather short path-length of ACK electrons, it is necessary for Gd atoms to be localized in the immediate proximity of DNA, i.e. within the nucleus¹. When an ACK electron is

emitted, it most likely will interact with a water molecule within a radius of a few nanometers producing a hydroxyl radical, which in turn locally propagates the oxidative damage¹². Lethal double-strand DNA breaks occur in proportion to the extent of the radiation-induced oxidative damage.

Intranuclear Gd detection with synchrotron spectromicroscopy

Conventional techniques such as fluorescence microscopy or autoradiography cannot detect Gd-DTPA or Gd-DOTA. We therefore used synchrotron spectromicroscopic methods to determine the intracellular and intranuclear localization of Gd. Spectromicroscopic techniques have now been used for more than a decade for elemental and oxidation-state analysis in magnetic^{13,14}, tribological¹⁵, environmental^{16–19} and catalysis²⁰ systems. Experiments in biology performed with hard-X-ray fluorescence imaging²¹ demonstrate excellent elemental sensitivity, but limited spatial resolution, while full-field soft-X-ray transmission microscopy achieves lateral resolution in the nanometer range, but lacks elemental sensitivity^{22,23}. Scanning transmission X-ray microscopy (STXM) and secondary ion mass spectrometry (SIMS) have been the only approaches to achieve both high resolution and chemical sensitivity in cells and tissues^{24–27}. The X-ray PhotoElectron Emission (X-PEEM)²⁸ type of spectromicroscopy has now reached a state of maturity such that it can be effectively introduced into the biomedical field to address high resolution and elemental analysis problems at the forefront of medical research. Here, we present the first images of physiological elements at the subcellular level obtained with the SPHINX (Spectromicroscope for PHotoelectron Imaging of Nanostructures with X-rays^{29,30} and MEPHISTO (Microscope à Emission de PHotoélectrons par Illumination Synchrotrique de Type Onduleur³¹ instruments at the Wisconsin Synchrotron Radiation Center. With these instruments it is possible to investigate trace element biodistributions, such as gadolinium localization into cell nuclei for GdNCT, as well as all other physiological elements. The SPHINX and MEPHISTO X-PEEM results *in vitro* were reproduced, validated and confirmed using the STXM spectromicroscope on beamline 11.0.2 at the Berkeley-Advanced Light Source for Gd analysis^{26,27}.

MATERIALS AND METHODS

Glioblastoma cell culture and cell exposure to Gd compounds

For *in vitro* studies, we used the T98G³² and TB10 human glioblastoma cell lines. TB10 is a new tumor cell line, established and characterized in our laboratory. Details on tumor cell culturing and immuno-phenotyping of TB10 have been described elsewhere^{5,33,34}. We also used the C6³⁵ rat glioma cell line. Cells were grown on silicon wafers for X-PEEM spectromicroscopy, on 100 nm thick Si_3N_4 windows for STXM spectromicroscopy, and in Petri dishes for inductively coupled

plasma mass spectrometry (ICP-MS) analysis. During the culture and exposure period all cell lines were maintained in a humidified incubator at 37°C and grown in DMEM-F12 medium containing 10% fetal bovine serum, 1% penicillin and streptomycin, 1% non-essential amino acids. Subconfluent cultures were exposed to one of the magnetic resonance imaging (MRI) contrast agents: gadolinium-diethylene triamine pentaacetic acid (Gd-DTPA; Magnevist, Schering AG, Berlin, Germany) or gadolinium-tetraazacyclododecane-tetraacetic acid (Gd-DOTA; Dotarem, Guerbet, Roissy CdG Cedex, France). The exposure times were 0, 6, 12, 24, 48 and 72 hours (six time points), and the concentrations of Gd compounds are shown in Table 1. Control dishes were treated with the same amount of the vehicle alone.

After exposure to the Gd compounds, the cell cultures on silicon substrates for X-PEEM analysis were washed three times with PBS solution to remove free Gd, fixed in 4% para-formaldehyde in PBS for 20 minutes, double washed in Milli-Q-water, air dried, and ashed in UV/O₃ for 140 hours³⁶. Parallel cultures were run and treated identically for ICP-MS measurements of the bulk Gd concentration. Each set of six samples (one per time point, 0, 6, 12, 24, 48 and 72 h exposure to 18 mM Gd-DTPA or 18 mM Gd-DOTA) was repeated in quadruplicate, from different cell passages. Cell cultures for STXM analysis on Si₃N₄ windows were exposed to 100 µM Gd-DTPA or 100 µM Gd-DOTA in the culture medium for 72 h, fixed, washed and air dried. Each sample was prepared in quadruplicate, although at the end of cell culturing and transportation to Berkeley only one sample per type had an intact Si₃N₄ window, and could be analyzed.

INDUCTIVELY COUPLED PLASMA MASS SPECTROMETRY (ICP-MS)

ICP-MS is a technique to measure total or bulk concentrations in any given solution. For the *in vivo* experiments, the volume of each tissue block was

accurately measured, followed by digestion in a known volume of 1 N HNO₃. The total amount of Gd was measured using ICP-MS and the results were normalized to the tissue volume. For *in vitro* cell cultures, the volume measurement is extremely inaccurate, and leads to >100% errors in the final analysis of Gd concentration in cells. We therefore counted the number of cells in a small aliquot from each culture, and calculated the total number of cells present in the sample (typically 2–7 × 10⁵ cells/sample). The cell volume was then calculated knowing the average volume of cells for each cell line. These were 62,400 TB10 cells/µl, 74,400 T98G cells/µl, and 98,000 C6 cells/µl. Once the accurate cell volume in each sample was extracted using these numbers, the ICP-MS results could simply be normalized (typical volume of cells 20–60 µl/sample). This strategy gave reproducible results across four repeated cultures, with errors usually within 30% (Table 1).

INTRACEREBRAL INJECTION OF C6 CELLS AND MAGNETIC RESONANCE IMAGING OF RAT TUMORS

The following experiments were performed in accordance with the animal care protocol approved by the Ethics Committee of the Catholic University of Rome, and of the University of Wisconsin-Madison Research Animal Resources Center (RARC)³⁷. Malignant rat C6 glioblastoma cells were used for intracerebral transplantation in rats. Adult male Wistar rats (200–250 g) (Catholic University Breeding Laboratory, Rome, Italy) were anesthetized with intraperitoneal diazepam (Valium, 2 mg/100 g; Roche, Milan, Italy) followed by intramuscular ketamine (Ketalar, 4 mg/100 g; Parke-Davis, Milan, Italy). The animal skulls were immobilized in a stereotactic head frame, and a burr hole was made 3 mm right of the midline and 2 mm behind the coronal suture. The tip of a Hamilton microsyringe was placed at a depth of 4 mm from the dura in the anterior caudate nucleus and the cells were slowly injected. Five hundred thousand cells in 5 µl medium with 10% fetal

Table 1: Exposure of Gd-compounds

Exposure compound	Cell line	Exposure concentration	[Gd] concentration in culture medium (ppm)	Exposure time (h)	[Gd] in cells ± SD (ICP-MS) (ppm)
Gd-DTPA	TB10	18 mM	2880	0–72	0–2260 ± 1213
Gd-DTPA	T98G	500 µM	80	0–72	0–862 ± 338
Gd-DTPA	T98G	100 µM	16	0–72	0–136 ± 29
Gd-DTPA	C6	500 µM	80	0–72	0–674 ± 216
Gd-DTPA	C6	100 µM	16	0–72	0–134 ± 34
Gd-DOTA	TB10	18 mM	2830	0–72	0–5067 ± 1051
Gd-DOTA	T98G	500 µM	80	0–72	0–136 ± 13
Gd-DOTA	T98G	100 µM	16	0–72	0–30 ± 10
Gd-DOTA	C6	500 µM	80	0–72	0–127 ± 28
Gd-DOTA	C6	100 µM	16	0–72	0–34 ± 2

The experimental paradigms used for the *in vitro* study. Exposure compound, cell line, exposure concentrations are reported. Six exposure times per cell culture were used, between 0 and 72 hours. The formula weights used for [Gd] exposure calculations for Gd-DTPA and Gd-DOTA are FW=546 g/mol and 577 g/mol, respectively. The last column shows Gd concentrations obtained with ICP-MS in cells (1 ppm=1 µg/ml≈1 µg/g). All uptake curves were similar, therefore results are reported only for the 72 h time points. All results were reproduced across three or four independent cell cultures, and the standard deviation is given in the last column.

calf serum (Gibco BRL, Life Technologies Italia, Milano, Italy) were injected in each rat. Ten days after surgery, the rats were anesthetized and treated with Gd-DOTA (Dotarem, 4×10^{-4} mol/kg; Guerbet, Roissy CdG Cedex, France) via tail vein injection. The dose of Gd-DOTA used in this experiment is two-fold the maximum recommended dosage when using this compound as MRI contrast agents in patients with brain tumors³⁸. Fourteen rats were injected with Gd-DOTA once or twice, with the second injection 12 hours after the first. One hour after the last Gd injection, the rats were killed with an overdose of barbiturate. In six rats, a region that included the tumor and 2 mm of surrounding tissue was dissected, immersed in OCT and flash-frozen in liquid nitrogen. For X-PEEM spectromicroscopy analysis, the frozen tissues were microtomed to 4 μ m thick sections, deposited on a silicon wafer, fixed overnight in paraformaldehyde vapors, and ashed for 108 hours. Adjacent sections were deposited on a glass slide, stained with hematoxylin and eosin (H&E), and analyzed for histology. The remaining portion of each tissue block was dissolved in 1 N HNO₃ and analyzed with ICP-MS.

In eight additional rats, magnetic resonance imaging of formaldehyde-fixed brains was obtained 48 hours after brain removal using a 1.5-tesla whole-body MR scanner (Horizon Echospeed, GE Medical System, Milwaukee, WI). The brains were kept in a plastic tube containing formaldehyde solution and maintained in the same position throughout imaging. Multi-slice coronal T1-weighted spin-echo images (TR 500 milliseconds, TE 17 milliseconds, NEX 3, field of view 12×9 cm², slice thickness 1.5 mm, space interval 0.2 mm) were acquired. Then, a T2-weighted spin-echo MR image was obtained (TR 4000 ms, TE 104 ms, NEX 3, field of view 12×9 cm², slice thickness 1.5 mm, space interval 0.2 mm) in the same slice positions. After MRI, the brains were embedded in paraffin, sectioned at 10 μ m on the coronal plane, and stained with H&E.

Human glioblastoma tumor sample preparation

Six GBM patients, scheduled for craniotomy and GBM resection at the Institute of Neurosurgery, Catholic University School of Medicine, Rome, gave informed consent³⁹ to the injection of Gd-DTPA (1×10^{-4} mol/kg; Magnevist, Schering, Milan, Italy) 1–2 hours before tumor excision. The tumor was immediately embedded in OCT, frozen in isopentane, and sectioned on a cryo-microtome at 4 μ m. Two adjacent tissue sections were collected from each tumor specimen. One section was deposited on a glass slide, fixed and stained with H&E for light microscopy. The adjacent section was deposited on a gold-coated silicon wafer, fixed in paraformaldehyde vapors, ashed, and studied with the MEPHISTO spectromicroscope.

X-PEEM spectromicroscopy analysis of cells and tissues

X-PEEM spectromicroscopy was performed both on C6 tumor specimens of rats injected with Gd-DOTA and on GBM tumor tissues from patients injected with

Gd-DTPA. The spectromicroscopy data on physiological elements as well as Gd distribution were obtained with either the SPHINX or MEPHISTO X-PEEM spectromicroscopes, installed on the HERMON beamline at the Synchrotron Radiation Center, and extracted according to the trace-element analysis strategy described at length elsewhere²⁹. SPHINX (Elmitec GmbH, Clausthal, Germany) and MEPHISTO (which we developed) have an optimum lateral resolution of 10 nm and 20 nm, respectively^{30,31}, and acquire X-ray absorption spectra with a resolving power up to 15,000 (E/ Δ E) in the 60–1300 eV energy range. For elemental distributions, the phosphorus map was obtained by digital ratio of images at 139 and 132 eV, on-peak and pre-peak of the P2p edge²⁹. A 5–10 μ m or 10–20 μ m diameter circular or elliptical region with high P signal was identified as the cell nucleus in rat and human tissues, respectively, and outlined for Gd intra-nuclear analysis. The nucleus is in fact rich in P due to the high density of phosphate groups in DNA. The Ca map was obtained dividing an image at 349 eV by one at 346 eV (Ca2p, on- and pre-peak, respectively). For C1s we ratioed 287 and 282 eV images, for K2p 297 and 295 eV, and for Na1s 1068 and 1059 eV images. For trace concentration Gd analysis, Gd-containing-pixel maps were obtained from stacks of 81 images across the Gd3d absorption edge at 1175 eV, and Gd peak areas were extracted from each pixel. This approach is preferable to the digital image ratio described for physiological elements, to produce distribution maps of elements occurring in trace amounts with lower noise and artifacts^{29,30}. Stacks of images, or 'Gd-movies', acquired between 1220 and 1140 eV, were binned 4×4 (therefore the resolution of the Gd map is four times lower than in the images, Gd pixel size = $1.4 \times 1.4 = 2$ μ m²) to enhance the Gd signal/noise ratio, and a Gd3d spectrum was extracted from each pixel. We then masked the Gd peak region, fitted the spectrum to a 7th order polynomial, divided the spectrum by the fitted curve, and obtained the Gd peak area, which is proportional to the local Gd concentration. We then displayed the Gd peak area in spectrum colors, and superimposed this map on a direct image of the cells or tissues.

Each Gd-movie was repeated twice, and only the reproducible Gd-pixels were retained as Gd-containing. Quantitative Gd concentration analysis with SPHINX or MEPHISTO is not possible at present. However, by maintaining all experimental and digital analysis parameters constant, the relative concentration of different Gd compounds in cells and tissues can be directly compared. From reference standards we estimate that this spectromicroscopy trace-element analysis has a minimum detection limit of <1000 ppm. Cell and tissue ashing increases [Gd] by a factor of 10, therefore the detection limit is on the order of 100 ppm or lower in all samples analyzed here. Since this detection limit is greater than the Gd concentration necessary for GdNCT (2.4 ppm or 13 ppm; see Discussion), in our analysis we accepted one Gd-containing pixel/nucleus as a sufficient amount for GdNCT²⁹. For both *in vitro* and *in vivo* experiments we identified the cell nuclei from the P distribution map,

counted the number of cell nuclei containing at least 1 Gd pixel, and evaluated the effectiveness of each Gd compound accordingly. Due to the time-consuming nature of the X-PEEM Gd data collection and processing, and also due to its low sensitivity, for *in vitro* experiments, only TB10 cells exposed to the two compounds for 0–72 h at the greatest concentrations were analyzed. For these, the bulk concentration reached 2000 ppm for Gd-DTPA and 5000 ppm for Gd-DOTA (see *Table 1*). Ashing in UV/O₃ selectively removes carbon, a major element in cells and tissues, and consequently enhances the relative concentration of the other elements. Ashing takes place at air pressure and temperature, and slowly (100–200 hours) ‘flattens’ the cell morphology³⁶. It is particularly useful when the element to be localized by X-PEEM is present in trace concentrations, otherwise undetectable.

STXM spectromicroscopy analysis of *in vitro* cell cultures

Due to the use of an undulator source, and the optimization of beamline 11.0.2 at the ALS for the Gd3d absorption energy (~1200 eV), the STXM spectromicroscope is much faster than X-PEEM for Gd detection, and much more sensitive. This instrument can in fact detect a single monolayer of Gd atoms. Ashing of the cell cultures for STXM analysis, therefore, was not required, and the exposure concentrations could be kept low, at 100 μM Gd-DTPA and Gd-DOTA. In addition, higher resolution in Gd and cell imaging was also possible on this novel instrument, designed and developed by one of us (T.T.) and his team^{26,27}. For Gd detection in cells we acquired images on- and off-peak, at 1183 eV and 1178 eV, respectively, then ratioed these two images to obtain the Gd distribution map, and superimposed it upon one of the sample images. Although this instrument does not allow the detection of P for nuclei identification, the nuclei appear thicker and denser in transmitted X-rays and, therefore, their outlines are easily located.

RESULTS

X-PEEM spectromicroscopy: physiological elements in cultured GBM cells

Despite the extensive manipulation, including fixation, air drying and ashing the samples, analysis of the morphology and elemental composition of cells demonstrated that we induced no elemental displacement at the detectable X-PEEM resolution, and that microanalysis of cells and tissues prepared with this modality is feasible. *Figure 1* shows the subcellular distribution of selected physiological elements in the TB10 human GBM cell line. Results indicate a higher concentration of P in cell nuclei, as expected, given the high density of phosphate groups in nucleic acids. The calcium map shows that the highest Ca concentration surrounds the nuclei, as anticipated, in the endoplasmic reticulum and Golgi apparatus. We observed a low concentration of carbon in the central region of each cell, which represents residual carbon not completely removed by

ashing. Potassium and sodium maps exhibited higher noise, corresponding to the lower concentrations of these elements compared with P and Ca. Neither P nor Ca were observed on the substrate, supporting the notion that elements were not re-distributed during ashing.

X-PEEM and STXM spectromicroscopy results: Gd distribution in cultured GBM cells

Both Gd-DTPA and Gd-DOTA are widely used MRI contrast agents that transiently ‘enhance’ GBM tumors as a result of a disrupted blood–brain barrier. We recently analyzed several GBM cell culture samples exposed to Gd-DTPA⁵ and found that Gd actually penetrates the nucleus *in vitro*. Encouraged by these results, we extended our research to include Gd-DOTA and analyzed more extensively the Gd-DTPA biodistribution, in the attempt to optimize the choice of Gd compounds for GdNCT.

In *Figure 2*, we show representative results of the intracellular distribution of Gd-DTPA and Gd-DOTA in cultured tumor cells. Following exposure to Gd-DTPA, Gd was found both in the nucleus and in the cytoplasm (*Fig. 2a*), but the Gd concentration was higher in nuclei (predominantly green vs. yellow, orange and red pixels). After exposure to Gd-DOTA, intracellular Gd was present at higher concentration as compared with Gd-DTPA (magenta and blue pixels in *Figure 2B*). It is strikingly apparent from the Gd location map of *Figure 2b* that Gd-DOTA is often excluded from the nuclei, at least within the sensitivity limit of SPHINX. The pixel value (color) indicates a locally higher Gd signal for the Gd-DOTA sample, in agreement with the bulk concentrations reported in *Table 1*.

Evaluation of Gd maps for the presence of at least one Gd pixel in the nucleus showed that at the 72-hour time point, Gd-DTPA was found in 84% of the nuclei in 76 cells analyzed, and Gd-DOTA in 56% of the 91 nuclei analyzed. Both results were collected across four independent cell cultures from different passages.

STXM analysis of TB10 and T98G cells exposed to 100 μM Gd-DTPA and 100 μM Gd-DOTA confirmed and validated these results. *Figure 3* shows the STXM image of two TB10 cells exposed to Gd-DOTA and imaged at 1183 eV, and the corresponding Gd distribution map. The distribution map shows most Gd pixels surrounding the cell cytoplasm, but also in the nucleus, particularly in the nucleoli. Overall we found Gd in eight of the 16 TB10 cells, and in 12 of the 20 T98G cells exposed to Gd-DOTA and analyzed with STXM. These correspond to 50% and 60%, respectively, of the nuclei containing Gd after exposure to Gd-DOTA. These numbers closely resemble the results found with X-PEEM (56%). STXM data (not shown) on TB10 cells exposed to Gd-DTPA showed Gd always present in higher concentration in the nucleus than in the surrounding cytoplasm. Twenty-four of the 28 cells imaged contained Gd (86%), which closely matches the X-PEEM result (84%). For both compounds, therefore,

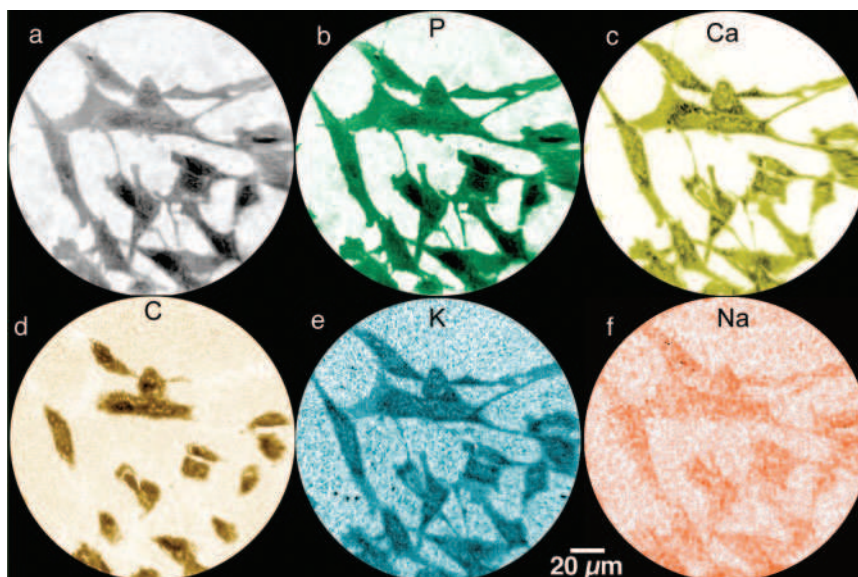


Figure 1: (a) Image of human GBM cells acquired by X-PEEM spectromicroscopy, using the SPHINX instrument, with 1200 eV photon energy illumination. (b) Phosphorus, (c) calcium, (d) carbon, (e) potassium and (f) sodium distribution maps in the same cells. In all distribution maps, black or dark color indicate higher element concentration, white corresponds to no element

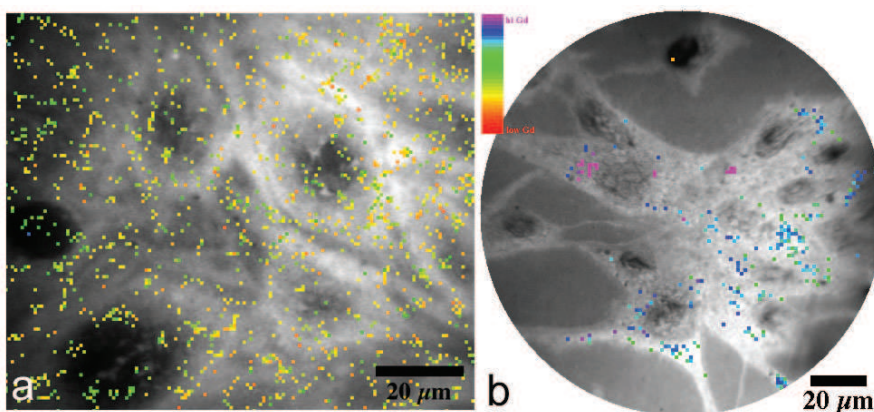


Figure 2: Gd-pixel location maps acquired with the MEPHISTO (a) and SPHINX (b) spectromicroscopes from human GBM TB10 cells exposed to (a) Gd-DTPA and (b) Gd-DOTA for 72 hours. The spectrum-color intensity scale indicates the highest Gd concentration in magenta, the lowest in red. Both Gd maps (pixel size $2 \mu\text{m}^2$) are fused on SPHINX grayscale images of the same cells. Nuclei are darker

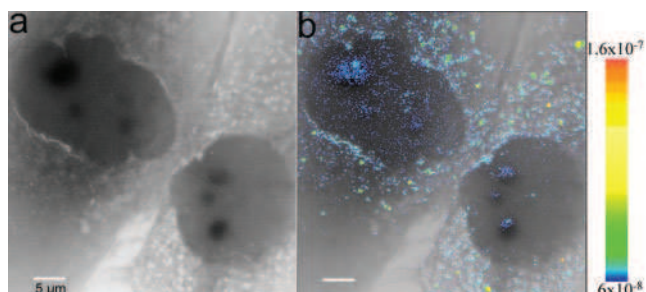


Figure 3: (a) Two TB10 cells exposed to Gd-DOTA and imaged with the STXM spectromicroscope at 1183 eV. (b) Gd map in the same cells, obtained by ratio of 1178 and 1183 eV images. Color bar values are estimated from Gd density and X-ray absorption measurements (in g/cm^2). The color Gd map is superimposed on the STXM image recorded at 1183 eV

X-PEEM and STXM spectromicroscopy data validate and corroborate each other.

Gd-DOTA in cells, analyzed with both spectromicroscopies, X-PEEM and STXM, shows that Gd accumulates with higher concentration and higher pixel density in the cytoplasm than in the nucleus (*Figures 2b* and *3b*). Exceptions to this observation are nucleoli: these are visible in $<10\%$ GBM cells, but when they are, they always contain a higher concentration of Gd, compared with the rest of the nucleus, but still lower than in the cytoplasm (e.g. *Figure 3b*).

The highest Gd pixel density and concentration, in the cytoplasm, is observed in discrete locations, or spots, in the perinuclear region. These could be subcellular organelles, or simply molecular aggregates of Gd-DOTA. We

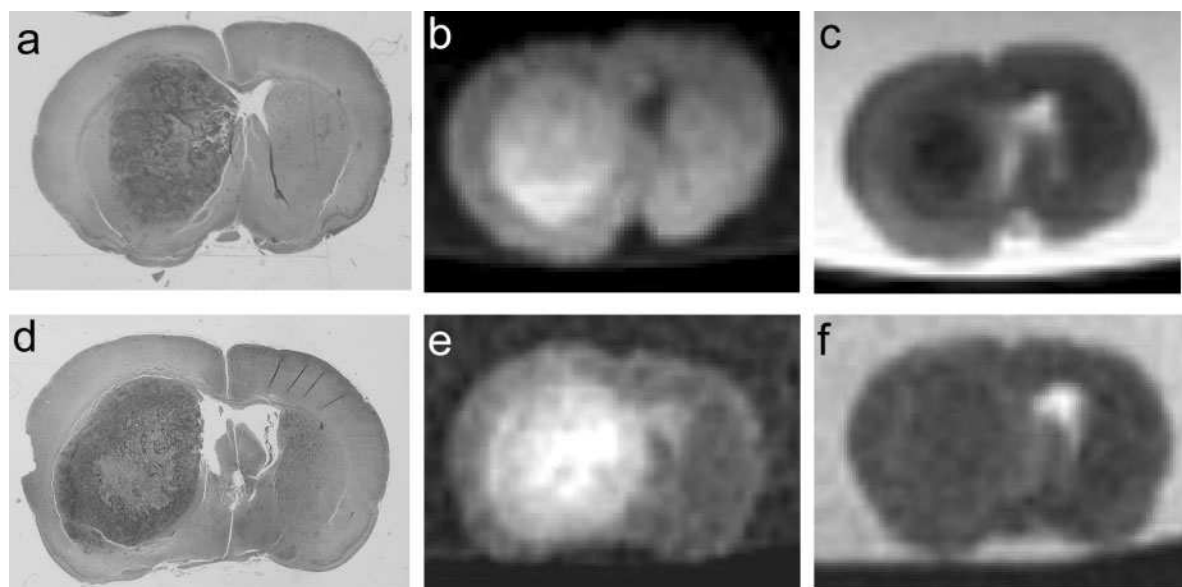


Figure 4: Histological and MRI studies of intracerebrally implanted C6 glioma tumor in rats. C6 cells were stereotactically injected in the right striatum. The upper panel (a, b, c) refers to a rat injected with a single dose of Gd-DOTA, the lower panel (d, e, f) to a rat injected with double dose of Gd-DOTA. (a) and (d) Coronal histological sections through the tumor epicenter stained with H&E (original magnification $\times 12.5$). (b) and (e) T1-weighted MRI images of the same specimens shown in (a) and (d). The tumors appear hyperintense after Gd-DOTA administration; however, some Gd enhancement is also localized in the edema region surrounding the tumor. In addition, the specimen with double Gd injection (e) shows a hyperintense signal, which highlights the profile of the cerebral ventricles. (c) and (f) T2-weighted MRI images of the same tissue specimen showing the typical hyperintense signal of the CSF in the ventricles

currently have no experimental proof supporting either interpretation. Analyzing only the nuclei found to contain Gd, we find very few of these Gd spots occurring at a much lower density than in the surrounding cytoplasm. It is conceivable that these are above the nucleus, in the cytoplasm, and the STXM experiment, which works in transmission, detects them in the nucleus. Similarly, in the X-PEEM experiment on ashed and flattened cells, if Gd was above the nucleus before ashing, it would appear in the nucleus after ashing. The cytoplasmic layer above the nucleus is considerably thinner than the portion surrounding the nucleus, which partially explains the lower number and density of spots we observe.

We note that the observation of highest Gd in the cytoplasm for Gd-DOTA and in the nucleus for Gd-DTPA eliminates the possibility of experimental artifacts or misinterpretations, such as cell surface-bound Gd.

MRI, ICP-MS and X-PEEM analysis of rat tumor tissues

All rats injected with Gd-DOTA showed intense signal enhancement in the brain identified as tumor in T1-weighted MR images. However, the area of signal enhancement was not restricted to the tumor itself but also included the surrounding brain tissue where peritumoral edema was identified on histological sections (Figure 4a,b). In addition, those rats receiving double Gd-DOTA injection showed presence of Gd in the cerebro-spinal fluid (CSF), as demonstrated by the hyperintense signal in the lateral ventricles on T1-weighted MR images (Figure 4e). This finding suggests

that diffusion of Gd to the extracellular space of the brain, which is in continuity with the CSF, did occur after repeated Gd-DOTA injections.

The ICP-MS results of Gd bulk concentration in rat tumors, after administration of Gd-DOTA are reported in Table 2. Comparison of SPHINX images with the adjacent histological sections confirmed that denser, darker regions (P-rich) corresponded to hematoxylin stained nuclei (Figure 5). On SPHINX analysis, Gd was homogeneously distributed throughout the tumor tissue and could be identified both in and between nuclei (Figure 5). Note that the distribution map of Gd appears so homogeneously random that it could be misinterpreted as noise. We carefully verified that each pixel corresponded to well-resolved Gd3d peaks, and that it was reproducible across two subsequent Gd movies.

Table 2 reports the overall results of the spectro-microscopy study at different sites that included the tumor itself, the peritumoral edema region, and normal brain tissue (Figure 6). In the tumor region, we found that Gd is present in 54 and 85% of cell nuclei after single and double Gd-DOTA injection, respectively (Table 2). In the case of double Gd-DOTA injection, however, we notice that Gd is present more frequently in cell nuclei of cells in the edema tissue than in tumor. Twelve hours after the second Gd-DOTA injection, there are still more Gd-containing nuclei in the region of brain edema than in the tumor itself. These findings suggest that in this rat the clearance of Gd-DOTA from edematous brain tissue may have been inhibited.

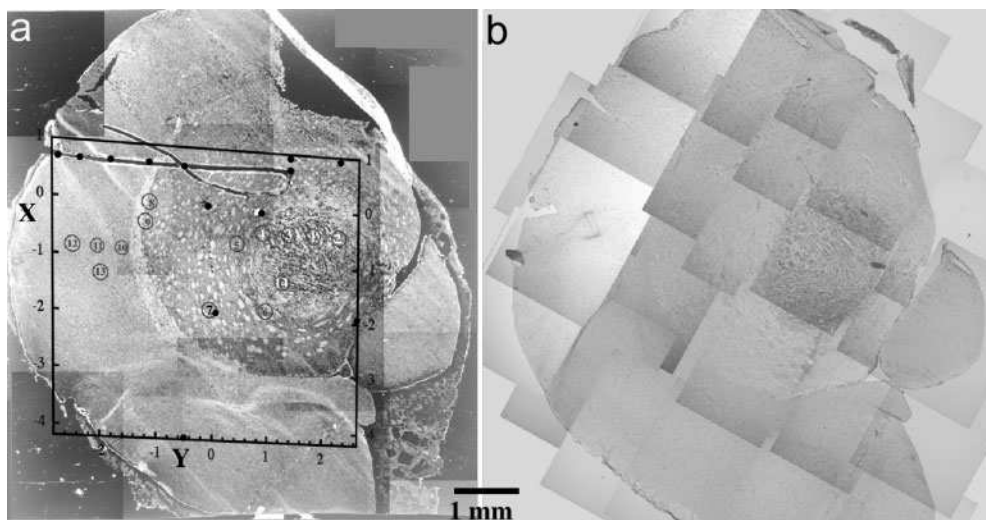


Figure 5: (a) Sample C61b on silicon, imaged in visible light after ashing and (b) the adjacent section H&E stained. The areas analyzed in SPHINX are indicated with circles. Black dots indicate distinctive features used to identify micro-locations and determine the correspondence of visible and SPHINX images. The resulting frame is also given, in which the X and Y coordinates accurately correspond to the SPHINX sample positioning micrometers

X-PEEM spectromicroscopy of Gd distribution in human GBM tissues

Figure 7 shows the results of the spectromicroscopic Gd analysis in human GBM tumor tissue. The Gd-pixel location was obtained using the same parameters as in Figures 2a,b and 6b, and the Gd concentrations can be directly compared. The same navigation system illustrated in Figure 5 allowed us to identify the areas in the two adjacent sections, so that the same portion of tissue could be examined for histology first (Figure 7a), and then imaged by MEPHISTO (Figure 7b). The phosphorus distribution map was superimposed on the MEPHISTO image to locate the cell nuclei, which are identified by the higher P concentration (Figure 7c). Systematic analysis of the tissue area in Figure 7, and a few more cells around it, showed that after a single injection of Gd-DTPA, Gd entered the nucleus of 12% of tumor cell nuclei (15 out of 123 cell nuclei). This is one of the most Gd-rich areas we identified. In Table 3 we report the results on all tissues analyzed. From Table 3 it is evident that the percentage of nuclei with Gd does not correlate with time between injection and tumor excision; but it correlates with the Gd

concentration measured by ICP-MS. This indicates, as expected, that the greater the concentration in GBM tissue, the greater the number of nuclei reached by Gd.

Overall, we analyzed 60 different circular areas, with diameter 200–300 μm , from all six patient tissues, and found that 6.1% of the cancer cell nuclei contained at least one Gd pixel (135 out of 2217). These data demonstrate that Gd, injected in the blood stream in the form of Gd-DTPA, reaches glioblastoma cells, and penetrates the cell and nuclear membranes. However, from the perspective of GdNCT, the nuclear localization of Gd from Gd-DTPA was unsatisfactory because only 6.1% of the nuclei analyzed contained Gd.

Interestingly, this *in vivo* value falls on the curve obtained from *in vitro* studies, as shown in Figure 8.

DISCUSSION

Theoretical requisites for GdNCT efficacy

Although many authors pointed out that the long-range effects of the GdNC reaction should not be neglected⁴⁰

Table 2: ICP -MS and SPHINX analysis of rat tissues

Sample ID and description	[Gd] in tissue (ppm)	% nuclei containing Gd (total no. of nuclei analyzed)		
		Tumor	Edema	Normal brain
C6 1a (Gd1, extr. after 1 h)	56			
C6 1b (Gd1, extr. after 1 h)	42	54% (287 nuclei)	39% (67 nuclei)	24%(146 nuclei)
C6 2 (Gd1, extr. after 1 h)	38			
C6 3 (Gd2, extr. after 12 h)	61	47% (177 nuclei)	66% (32 nuclei)	Not available
C6 4 (Gd2, extr. after 12 h)	196			
C6 5 (Gd2, extr. after 1 h)	88	85% (266 nuclei)	91% (75 nuclei)	Not available
C6 6 (Gd2, extr. after 1 h)	57			

ICP-MS results obtained in tumors from six rats injected with Gd-DOTA. Samples 1a and 1b were extracted from the same rat. Gd1 indicates 1 injection, Gd2 indicates two injections, 12 hours apart. The three samples analyzed with SPHINX, and the corresponding results divided by tissue regions are reported in the three columns on the right.

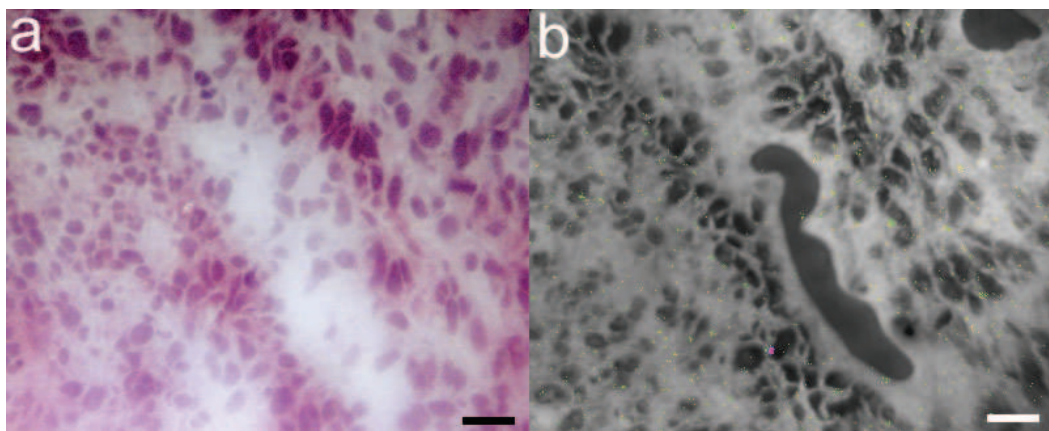


Figure 6: Two adjacent tumor tissue sections from a rat injected with Gd-DOTA and killed 1h later (C6-1b in Table 2). (a) A visible light image of the H&E stained section shows the density of nuclei in the GBM tumor. (b) SPHINX image of the same area in the adjacent section after ashing, which shows similar features. Superimposed on this image is the map of Gd-containing pixels and relative concentrations, displayed with the same spectral color palette of Figure 2. Bars=20 μm

intranuclear presence of Gd is key to the development of GdNCT. Before performing the present experiments on Gd microdistribution, our hypothesis was that one or more Gd-contrast agents might be identified as useful NCT agents as well, contingent upon uptake in at least 90% of the tumor cell nuclei. This criterion is based on a previous demonstration by Fowler *et al.* that if cytotoxicity is dependent on intracellular incorporation

of a test agent, the factor limiting its success is the proportion of tumor cells not incorporating the test agent, and therapeutic benefit is unlikely to be achieved if more than 10% of the cells remain unlabeled⁴¹. For GdNCT, one or two neutron capture events close to DNA would be sufficient to kill a cell; however, enough Gd molecules should be present in the nucleus of virtually every malignant cell in order to achieve a

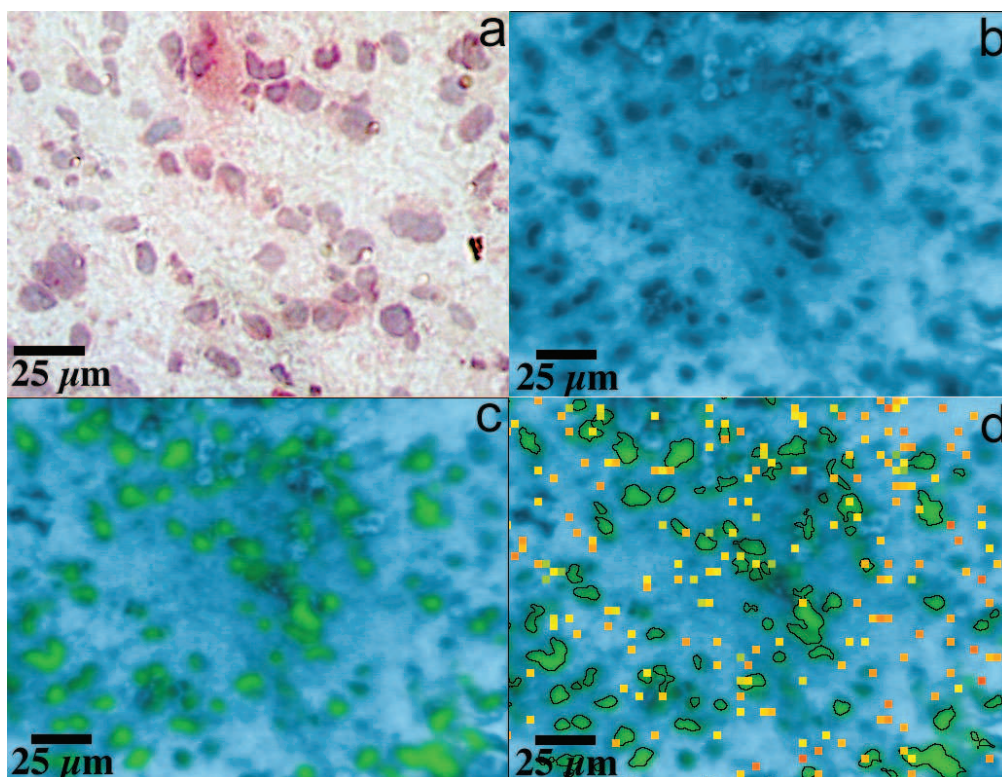


Figure 7: (a) Light microscopy image of a human glioblastoma tissue section stained with H&E from sample #35 in Table 3. (b) MEPHISTO image of the same region as in (a) obtained at 130 eV photon energy. (a) and (b), acquired on two adjacent tissue sections, are similar but not identical because the tissue sections are 4 μm thick while the size of the nuclei is 5–10 μm. (c) Phosphorus distribution map, in green, to outline the cell nuclei. (d) Gd-location map, superimposed on the outlined cell nuclei

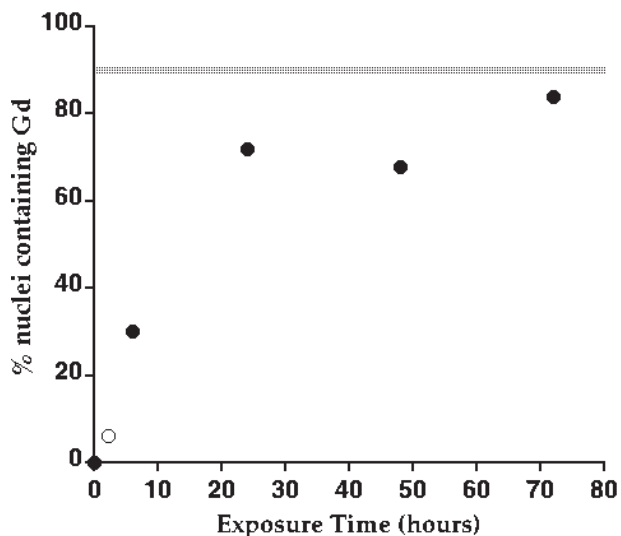


Figure 8: Diagram showing the relationship between the percentages of nuclei in which Gd was detected, as in Figure 2a, and the time of exposure of GBM cells to Gd-DTPA (solid circles). In the human GBM cases injected with Gd-DTPA (empty circle at the average 2.2 hour, 6.1% nuclei), the value falls onto the *in vitro* curve

therapeutically relevant effect. The amount of Gd necessary for GdNCT efficacy can be calculated from the formula:

$$\# \text{ GdNC event} = n \Phi \sigma$$

where # GdNC events=number of Gd neutron capture events/nucleus; n =number of Gd atoms/nucleus; Φ =neutron fluence= $10^9 \text{ n/cm}^2\text{s} \times 3\text{h} = 1.1 \times 10^{13} \text{ n/cm}^2$, which is clinically feasible⁴²⁻⁴³, and $\sigma = ^{157}\text{Gd}$ absorption cross-section for thermal neutrons= $254,000 \text{ barn} = 0.25 \times 10^{-18} \text{ cm}^2$.

One neutron capture/nucleus can be achieved if 4×10^5 Gd atoms/nucleus are present, which corresponds to $[\text{Gd}] = 0.1 \text{ ppm}$. Two of us (J.F.F. and J.F.C.) independently calculated that, assuming a Poisson distribution of Gd molecules in cell nuclei as a result of uptake from the vasculature, there must be an average of at least 24 GdNC events per nucleus

($[\text{Gd}] \cong 2.4 \text{ ppm}$ in the nucleus, or, using the natural Gd isotopic mixture with $\sigma = 49,000 \text{ barn}$, $[\text{Gd}] \cong 13 \text{ ppm}$), in order to be sure that less than one in the 10^{10} cells/tumor has zero events.

Although quantitative X-PEEM spectromicroscopic analysis is not yet available, from a comparison with the ICP-MS bulk concentrations, we estimate that the detection limit is on the order of 1000 ppm in ashed cells. Therefore, if we detect Gd in one pixel, that pixel area ($2 \mu\text{m}^2$) must have contained at least 100 ppm Gd in the cell before ashing, which is sufficient for GdNCT, and well above the modeled average of 13 ppm for GdNCT efficacy. Our goal is, therefore, the detection of at least one Gd spot in the nucleus of at least 90% of the tumor cells.

In the human *in vivo* experiments, however, we found that only 6.1% of the cell nuclei contain Gd pixels after one single injection of Gd-DTPA. Cell culture experiments might offer a way to compare *in vivo* and *in vitro* data. Figure 8 shows the nuclear uptake of Gd in cultured GBM cells exposed to Gd-DTPA as a function of exposure time. In this diagram, the percentage of Gd nuclear uptake in the *in vivo* condition falls onto the uptake curve obtained *in vitro* as a function of time, when one assumes that (a) the time between injection and surgical tumor removal corresponds to the exposure time, (b) the blood concentration of Gd remains constant over this time. Although the calculation of $[\text{Gd}]$ in the blood supplying the tumor might suffer from inaccurate assumptions, we estimate this value to be $\sim 124\text{--}132 \text{ ppm}$. In the *in vitro* study, the exposure concentration for cells was 18 mM or 10 mg/ml Gd-DTPA, which corresponds to $[\text{Gd}] = 2880 \text{ ppm}$. Therefore, in the *in vivo* conditions, the $[\text{Gd}]$ in blood is well below the $[\text{Gd}]$ in the culture medium.

Hypothetically, by extending the time of Gd exposure, the nuclear uptake *in vivo* might significantly increase. Longer exposure times can be reproduced *in vivo* by continuous infusion or multiple administrations of Gd compounds to patients. The experience with GBM and brain metastases patients demonstrates that multiple administrations of a different Gd compound,

Table 3: *In vivo* human cases injected with 30 mg/kg Gd-DTPA

Sample ID	Time between injection and tumor excision (h)	ICP-MS $[\text{Gd}] \pm \text{St. Dev.}$ (ppm)	MEPHISTO analysis: areas with Gd/analyzed areas (%)	MEPHISTO analysis: nuclei with Gd/analyzed nuclei (%)
# 35	1	10.0 ± 2.0	4/11 (36)	48/406 (11.8)
# 37	2.5	9.0 ± 2.0	1/7 (14)	28/287 (9.7)
# 36	2	4.7 ± 0.9	1/6 (17)	17/182 (9.3)
# 40	2.5	1.8 ± 0.4	5/13 (38)	21/433 (4.8)
# 39	3	1.5 ± 0.3	4/14 (28)	14/458 (3)
# 38	2	0.6 ± 0.1	2/9 (22)	7/451 (1.6)
Average			17/60 (28)	135/2217 (6.1)

Gadolinium concentration in tumor tissue, extracted from six GBM patients injected pre-operatively with Gd-DTPA, measured by ICP-MS, and visualized by MEPHISTO spectromicroscopy. The MEPHISTO results of the fourth column represent the ratio of the 200–300 μm -diameter tissue areas in which Gd was observed over the total number of sections analyzed. The last column gives the number of nuclei in which Gd was found over the total number of nuclei analyzed for each patient (tissue section).

Motexafin-gadolinium (MGd), lead to intratumoral accumulation and retention even 2 months after the last administration⁴⁴. If the *in vitro*–*in vivo* correspondence of Figure 8 is reliable, one might extrapolate that after a 72-hour continuous infusion of Gd-DTPA to patients with GBM, 84% of the tumor cell nuclei would contain Gd, a value which approaches but still does not reach the goal of 90%. In general, if a Gd compound does not target a sufficient number of tumor cell nuclei *in vitro*, it is unlikely to do so *in vivo*. Furthermore, continuous or repeated Gd-infusions may lead to an excess of Gd in the blood stream at the time of neutron exposure, and undesirable side effects and complications.

Our *in vitro* studies with Gd-DOTA showed that the potential of Gd-DOTA as GdNCT agent is not greater than for Gd-DTPA. After cell exposure to 18 mM Gd-DOTA for 72 hours, only 56% of the cell nuclei contained Gd. *In vivo*, the percentage of nuclei containing Gd varied between 47% and 85% after single or double injection of Gd-DOTA, respectively. Thus, with repeated Gd-DOTA injections, a higher percentage of nuclei did contain Gd. However, repeated Gd-DOTA injections resulted in Gd extravasation in the CSF as well as in the edematous white matter surrounding the tumor, as demonstrated both by MRI and spectromicroscopy. This may have relevant pathological effects following neutron irradiation, such as ependymitis or radionecrosis.

Comparison of X-PEEM and STXM *in vitro* data reveals an unexpected result: the percentage of nuclei with Gd may not depend on the exposure concentration. The latter was 18 mM and 100 μ M for X-PEEM and STXM experiments, respectively, for both Gd compounds. Despite this significant difference, the percentage of nuclei taking up Gd after 72 hours did not vary significantly across the two experiments. However, this observation may be hindered by the difference in sensitivity of the two techniques, and cannot at this time lead to any further conclusions.

In conclusion, GdNCT had been previously abandoned because evidence for intracellular and intranuclear Gd localization was lacking. There is now a strong motivation for revisiting GdNCT, since it became possible to analyze the intracellular Gd localization in detail, and to evaluate the uptake and biodistribution of Gd compounds before clinical testing. Our unprecedented *in vitro* and *in vivo* Gd spectromicroscopy data in human and rat glioma tumors provide evidence that neither Gd-DTPA nor Gd-DOTA are suitable agents for GdNCT, since these compounds do not target a sufficient number of tumor cell nuclei. Despite the rejection of these agents, our results validate the authenticity, reproducibility and versatility of the spectromicroscopy approach to determine the biodistribution of Gd *in vitro* and *in vivo*. In the future, when another GdNCT agent, targeting >90% of tumor cell nuclei, is identified with spectromicroscopy, pre-clinical animal and early clinical testing with thermal and epithermal neutron irradiation should proceed to determine the efficacy of GdNCT.

ACKNOWLEDGEMENTS

This work was supported by the University of Wisconsin Comprehensive Cancer Center, UW-Graduate School Romnes Award and Department of Physics. X-PEEM spectromicroscopy experiments were conducted at the UW-Synchrotron Radiation Center, supported by the NSF under Award No. DMR-0084402. The ALS and work on the beamline 11.0.2 STXM is supported by the Director, Office of Science, Office of Basic Energy Sciences, Division of Materials Sciences and the Division of Chemical Sciences, Geosciences, and Biosciences of the U.S. DOE at LBNL under Contract No. DE-AC03-76SF00098.

REFERENCES

- Martin RF, D'Cunha G, Pardee M, et al. Induction of DNA double-strand breaks by ¹⁵⁷Gd neutron capture. *Pigment Cell Res* 1989; **2**: 330–332
- Brugger RM, Shih JA. Evaluation of gadolinium-157 as a neutron capture therapy agent. *Strahlenther Onkol* 1989; **165**: 153–156
- Smith DR, Chandra S, Coderre JA, et al. Ion microscopy imaging of ¹⁰B from p-boronophenylalanine in a brain tumor model for boron neutron capture therapy. *Cancer Res* 1996; **56**: 4302–4306
- Masiakowski JT, Horton JL, Peters LJ. Gadolinium neutron capture therapy for brain tumors: a computer study. *Med Phys* 1992; **19**: 1277–1284
- De Stasio G, Casalbone P, Pallini R, et al. Gadolinium in human glioblastoma cells for gadolinium neutron capture therapy. *Cancer Res* 2001; **61**: 4272–4277
- Goorley T, Nikjoo H. Electron and photon spectra for three gadolinium-based cancer therapy approaches. *Radiat Res* 2000; **154**: 556–563
- Powell CJ, Jablonski A. NIST Electron Inelastic-Mean-Free-Path Database – Version 1.1, 2000; National Institute of Standards and Technology, Gaithersburg, MD
- Greenwood RC, Reich CW, Baader HA, et al. Collective and two-quasiparticle states of ¹⁵⁸Gd observed through study of radiative neutron capture in ¹⁵⁷Gd. *Nucl Phys* 1978; **A304**: 327–428
- Gierga DP, Yanch JC, Shefer RE. An investigation of the feasibility of gadolinium neutron capture synovectomy. *Med Phys* 2000 **27**: 1685–1692
- Miller GA, Hertel NE, Wehring WB, et al. Gadolinium neutron capture therapy. *Nucl Technol* 1993; **103**: 320–331
- X- and gamma-ray mass attenuation coefficients and distances in brain were retrieved from the NIST tables available at: <http://physics.nist.gov/PhysRefData/XrayMassCoef/ComTab/brain.html>
- Hall EJ. DNA strand breaks and chromosomal aberrations. In: *Radiobiology for the Radiologist*, 5th edn, Philadelphia: Lippincott Williams & Wilkins, 2000; pp. 19–20
- Scholl A, Stöhr J, Lüning J, et al. Observation of antiferromagnetic domains in epitaxial thin films. *Science* 2000; **287**: 1014–1016
- Stöhr J, Wu Y, Hermsmeier BD, et al. Element-specific magnetic microscopy with circularly polarized x-rays. *Science* 1993; **25**: 658–661
- Canning GW, Suominen Fuller ML, Bancroft GM, et al. Spectromicroscopy of tribological films from engine oil additives. Part I. Films from zddp's. *Tribology Lett* 1999; **6**: 159–169
- Chan CS, De Stasio G, Banfield JF, et al. Microbial polysaccharides template assembly of nanocrystal fibers. *Science* 2004; **303**: 1656–1658
- Labrenz M, De Stasio G, Banfield JF et al. Formation of sphalerite (ZnS) deposits in natural biofilms of sulfate-reducing bacteria. *Science* 2000; **290**: 1744–1747
- Beard BL, Johnson CM, Cox L, et al. Iron isotope biosignatures. *Science* 1999; **285**: 1889–1892
- Feng X, Fryxell GE, Wang L-Q, et al. Functionalized monolayers on ordered mesoporous supports. *Science* 1997; **276**: 923–926
- Rotermund HH, Engel W, Kordesch M, Ertl G. Imaging of spatiotemporal pattern evolution during carbon-monoxide oxidation of platinum. *Nature* 1990; **343**: 355–357
- Pickering IJ, Prince RC, Salt DE, et al. Quantitative, chemically specific imaging of selenium transformation in plants. *Proc Natl Acad Sci USA* 2000; **97**: 10717–10722
- Larabell CA, Le Gros MA. X-ray tomography generates 3-D reconstructions of the yeast, *Saccharomyces cerevisiae*, at 60 nm resolution. *Mol Biol Cell* 2003; **15**(3): 957–62

- 23 Myneni SCB, Brown JT, Martinez GA, et al. Imaging of humic substance macromolecular structures in water and soils. *Science* 1999; **286**: 1335–1337
- 24 Osanna A, Jacobsen C, Kalinovsky A, et al. X-ray microscopy: preparations for studies of frozen hydrated samples. *Scanning Microsc* 1996; **10** (suppl.): 349–356
- 25 Smith DR, Chandra S, Barth RF, et al. Quantitative imaging and microlocalization of boron-10 in brain tumors and infiltrating tumor cells by SIMS ion microscopy: relevance to neutron capture therapy. *Cancer Res* 2001; **61**: 8179–8187, and the references therein
- 26 Kilcoyne ALD, Tyliczszak T, Steele WF, et al. Interferometer-controlled scanning transmission X-ray microscopes at the advanced light source. *J Synchrotron Rad* 2003; **10**: 125–136
- 27 Tyliczszak T, Warwick T, Kilcoyne ALD, et al. Soft X-ray scanning transmission microscope working in an extended energy range at the advanced light source. *AIP Conference Proceedings*, 2004; **705**: 1356–1359
- 28 Bauer E. Photoelectron microscopy. *E J Phys Cond Matter* 2001; **13**: 11391–11404
- 29 Frazer BH, Sonderegger BR, De Stasio G, et al. Mapping of physiological and trace elements with X-PEEM. Proceedings of the 2002 X-ray Microscopy Conference. *J Phys Fr IV* 2003; **104**: 349–352
- 30 Frazer BH, Girasole M, De Stasio G, et al. Spectromicroscope for the PHotoelectron Imaging of Nanostructures with X-rays (SPHINX): performance in biology, medicine and geology. *Ultramicroscopy* 2004; **99**: 87–94
- 31 De Stasio G, Perfetti L, Gilbert B, et al. The MEPHISTO spectromicroscope reaches 20 nm lateral resolution. *Rev Sci Instrum* 1999; **70**: 1740–1742
- 32 Stein GH. T98G: An anchorage-independent human tumor cell line that exhibits stationary phase G1 arrest in vitro. *J Cell Physiol* 1979; **99**: 43–54
- 33 Pallini R, Casalbore P, Mercanti D, et al. Phenotypic change of human cultured meningioma cells. *J Neuro-Oncol* 2000; **49**: 9–17
- 34 Falchetti ML, Pierconti F, Pallini R, et al. Glioblastoma induces vascular endothelial cells to express telomerase *in vitro*. *Cancer Res* 2003; **63**: 3750–3754
- 35 Albasanz JL, Ros M, Martin M. Characterization of metabotropic glutamate receptors in rat C6 glioma cells. *Eur J Pharmacol* 1997; **326**: 85–91
- 36 Gilbert B, Perfetti L, Hansen R, et al. UV-ozone ashing of cells and tissues for spatially resolved trace element analysis. *Front Biosci* 2000; **5**: 10–17. On-line at <http://www.bioscience.org/2000/v5/a/gilbert/fulltext.htm>
- 37 University of Wisconsin-Madison Research Animal Resources Center (RARC), Animal Protocol A-48-6700-M01613-4-03-02 approved 04/08/2002
- 38 www.biam2.org/www/Sp29085.html
- 39 University of Wisconsin, Institutional Review Board, Human Subjects Committee, approved Protocol # 2000-2127
- 40 Stalpers L, Stecher-Rasmussen F, Kok T, et al. Radiobiology of gadolinium neutron capture therapy. In: Sauerwein S, Moss R, Wittig A, eds, *Research and Development in Neutron Capture Therapy*, Bologna, Italy: Monduzzi, 2002: pp. 825–830
- 41 Fowler JF, Kinsella TJ. The limiting radiosensitisation of tumours by S-phase sensitisers. *Br J Cancer* 1996; **74** (Suppl. XXVII): S294–S296
- 42 Riley KJ, Binns PJ, Harling OK. Performance characteristics of the MIT fission converter based epithermal neutron beam. *Phys Med Biol* 2003; **48**: 943–958
- 43 Verbakel WFAR, Sauerwein W, Hideghety K, et al. Boron concentrations in brain during boron neutron capture therapy: *In vivo* measurements from the Phase I trial EORTC 11961 using a gamma-ray telescope. *Int J Radiat Oncol Biol Phys* 2003; **55**: 743–756
- 44 Mehta MP, Shapiro WR, Glantz MJ, et al. Lead-in phase to randomized trial of motexafin gadolinium and whole-brain radiation for patients with brain metastases: centralized assessment of magnetic resonance imaging, neurocognitive, and neurologic end points. *J Clin Oncol* 2002; **20**: 3445–3453